Please cite the Published Version

Publisher: The International Council of the Aeronautical Sciences

Version: Accepted Version

Downloaded from: https://e-space.mmu.ac.uk/637325/

SENECA'S AIRCRAFT EMISSIONS EVALUATION AND THEIRS ENVIRONMENTAL CONSIDERATIONS

Terrenoire[1]E., M. Muller[1], E. Ramirez Correra[2], P. Leyland[2], K. Synylo[3], A. Krupko[3], O. Zaporozhets[3,4], D. Lee[5], B.Owen[5], L. Lim[5], A. Skowron[5], R. Rodriguez De Leon[5], D. Marsh[5], S. Matthes[6], P. Madden[7],S. Bake[8], C. Mourouzidis[9]

[1]ONERA, (France)
[2]AEDS (Switzerland)
[3]NAU (Ukraine)
[4]ILOT (Poland)
[5]Manchester Metropolitan University (UK)
[6]DLR (Germany)
[7]Rolls Royce UK (UK)
[8]Rolls Royce DE (Germany)
[9]Cranfield University (UK)

mailto: etienne.terrenoire@onera.fr

Abstract

Keywords: supersonic, emission indexes, climate effects, NOx/H_2O, contrails.

1. INTRODUCTION

The SENECA[1] supersonic aircraft concepts and associated engines cover the two main categories: airliners of approximately 100 PAX with four engines and bizjets with two engines. The work presented here aims to assess the environmental impact of future fleets (2050) of such aircraft. This covers in particular: Airport mission pairs, with respective geographical and altitudinal distribution of flight patterns, with associated inventory of aircraft emissions. Emission indices of various types, such as NO_x, CO, CO_2 and SO_x are determined from the more detailed engine studies provided by the SENECA engine team. Contrail 3D characteristics are assessed along with a novel RANS/LES coupling approach allowing simulating the contrails during the jet and vortex phases. Finally, the emissions effects and associated radiative forcing of NOx on stratospheric and tropospheric ozone and water vapor are modelled with a variety of complex climate models.

2. ROUTE DEFINITION AND EMISSION INVENTORY

SENECA presents four supersonic aircrafts of two types: two bizjet (Cruise Mach 1.4 & 1.6), and 2 Airliner (Cruise Mach 1.8 & 2.2). The targeted range is 4000 nm. Supersonic flight is aimed to only be over water (with a buffer zone to land), and the option of refueling for longer missions if necessary is considered. Based on a forecast of demand extrapolated to 2050, airport pairs, possible supersonic routes are made. The emission inventory calculation uses MMU's FAST model used in many research programs and CAEP. From the engine data performance sheets along the complete mission (LTO with acceleration and cruise), the routes and the emission evaluations an inventory is generated.

3. EMISSION ESTIMATION

3.1 Kinetic modelling for Emission Indexes's (EIs) estimation

---

[1] (LTO) noiSe and EmissioNs of supErsoniC Aircraft (H2020 EU project)

Emission estimations are performed using coupled combustion kinetics for an assumed Jet A1 kerosene fuel, using quasi 0D model to describe the pollutants formation in combustor and quasi-1D model to describe non-equilibrium processes in the turbine and nozzle flow (gas dynamics and chemistry interactions). The main technique used follows a scheme using Chemical Reactor Network (CRN) models. The chemical kinetic reaction estimations coupling the reactor models and reaction kinetics are made using an open-source tool CANTERA [1].

The modelling workflow starts from the aero-engine geometrical and thermodynamic data, from which a zero- and one-dimensional (0D/1D) network is built. For every reactor, inlet temperature, pressure and composition must be defined, as well as the reactor volume for 0D reactors, or reaction area and length for 1D reactors. Both types are considered as ideal gas, constant pressure systems, with 0D being modelled as Perfectly Stirred Reactors (PSR) and 1D modelled as Plug Flow Reactors (PFR). Evolution of species is quantified by means of the corresponding balance equations, which include chemical kinetic terms. PSR and PFR reactors are the modules upon which the reactor network is built to emulate the combustion chamber of the SENECA aircraft engines. The Mach 1.8 airliner engine designed by DLR and the Mach 1.6 bizjet of Cranfield University (CU) are considered. The models developed are first calibrated and validated for the CFM56 7B27/B1F engine similarly to [2] and for the bizjet engine, on the HISAC generic engine [3].

For the Jet A1 fuel, three models for the reaction chemistry are considered. In a first step, [4] mechanisms (225 species, 1800 reactions) and a reduced version thereof [5] have been used (89 species, 680 reactions). In both cases, a kerosene surrogate has been defined as: 74% $C_{10}H_{22}$, 15% PHC_3H_7, 11% CYC_9H_{18}, where composition is in mole fraction. Additionally, sulphur chemistry has been added based on [6] and [7] works, where H_2S is used as sulphur surrogate in the fuel to simulate 400 ppm (in mass) sulphur content in kerosene. In a final step, collaborations with Sandia National Laboratories have given access to additional more detailed mechanisms [8] (861 species, 6074 reactions) and surrogates for Jet A1 fuel including sulphur content.

Using the bizjet M1.6 of CU's mission point's dataset, which consists of 267 operational points from take-off to acceleration to cruise and part of the descent, the modelling gives the following results. In Figure 1, EINOx and EICO are shown. It can be observed that regarding NOx emissions, there is a strong correlation with the fuel/air ratio, which is consistent with the findings also for the ICAO points, and specific design points which are defined as MCR (Mid Cruise), SS TOC (Supersonic Top of Climb), SS EoA (TP) (Supersonic End of Acceleration), EOR (End of Runway), and SLS (Sea Level Static). SO2 emissions is also shown, with EISO2 being close to 0.8 g/kg which is a reasonable result, given that sulphur primarily produces SO2 as a pollutant.
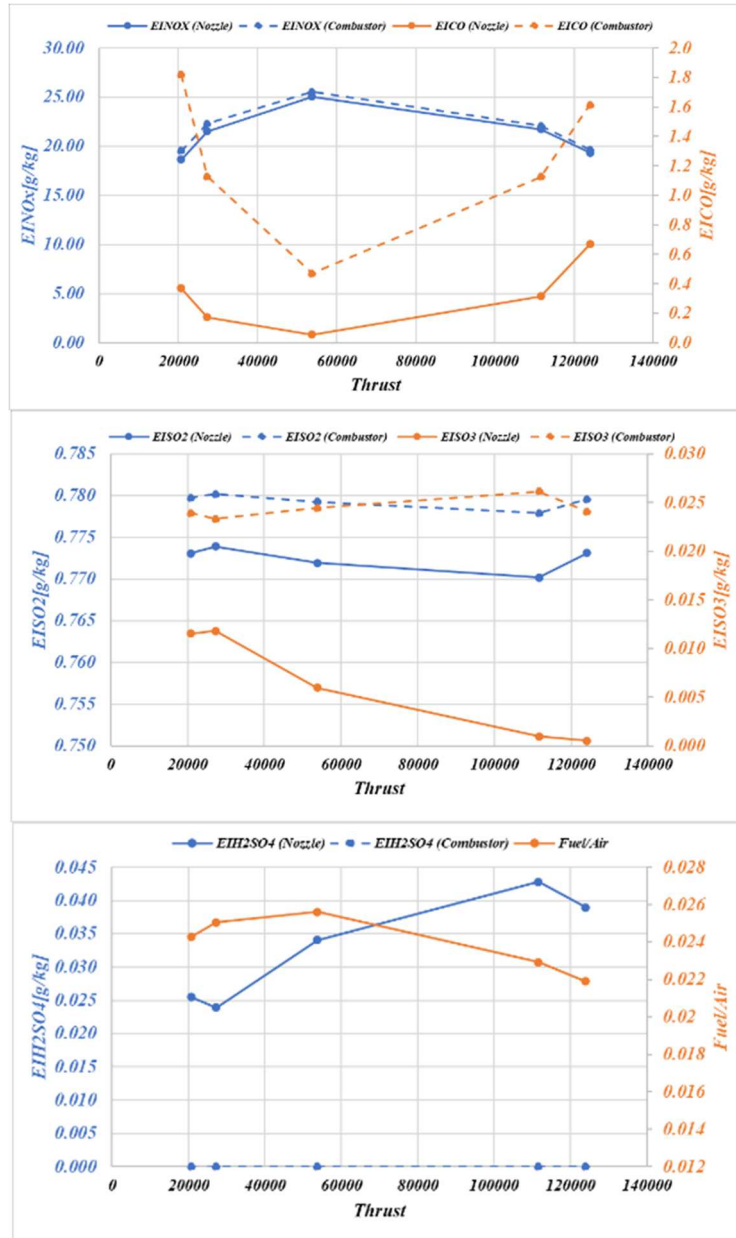
Figure 1: EINOx/EICO (top), EISO2/3 (middle and EISO3/UHC (bottom) kinetic method for the M1.6 bizjet

3.2 Correlation Methods for EI's calculation

Emission indices have also been calculated for business jet supersonic aircraft (Ma=1.6) using the P3T3 method [9, 10] for NOx (EINOx). The main performance parameters (temperature (T3) and pressure (P3) at combustion chamber inlet, fuel to air ratio) distribution across the mission profile were provided by the engine design of Cranfield University (CU). Additionally, the investigation results of ICAO LTO-cycle were provided by CU to estimate of EINOx at reference conditions (Figure 2).

Figure 2: The estimation of reference EINOx as function of T3 on the basis ICAO LTO cycle

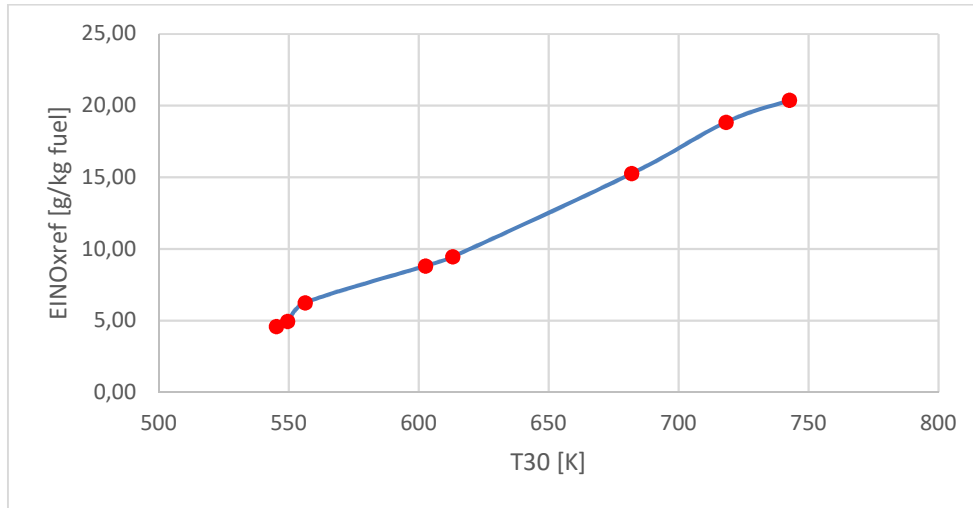The EINOx were calculated by the P3T3 method (module of complex model PolEmiCa) [Synylo 2018] for each of the four stages (take-off, subsonic climb, supersonic climb, supersonic cruise) of the flight profile, and compared to the values obtained with the method of AEDS in Figure 3. Distribution of meteorological parameters (temperature, pressure) were estimated in accordance with manual of the ICAO standard atmosphere [11]. Modelling of EI were implemented for two cases of relative humidity (30% and 60%). Analysis of the obtained results demonstrated, that the influence of relative humidity on emission indices is insignificant. Additionally, EINOx were calculated in accordance to NASA model [12], which is quite well correlated with P3T3 results.
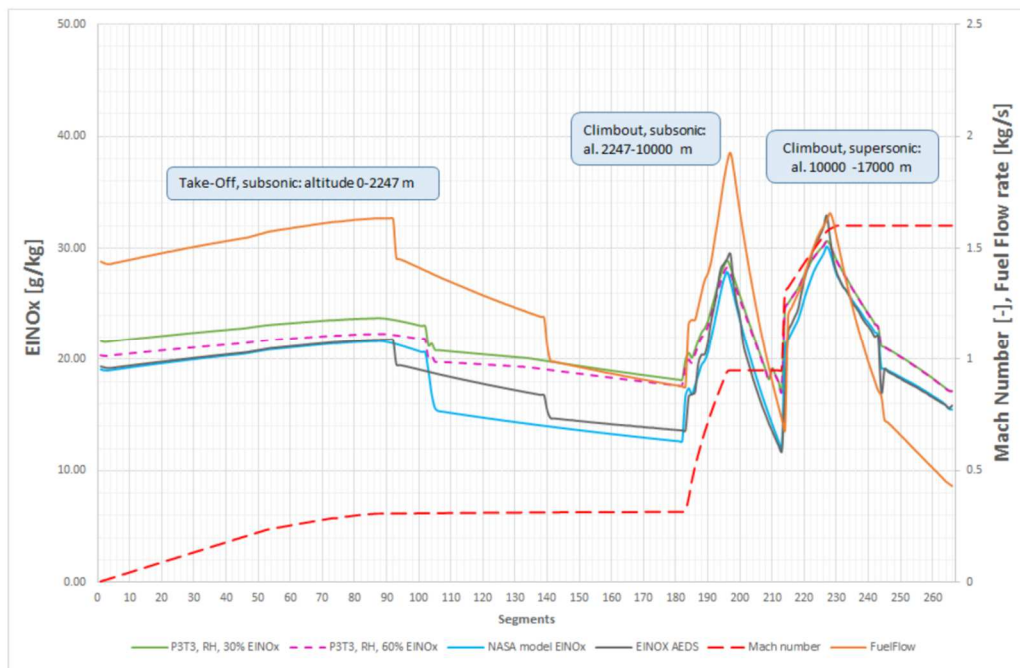
Figure 3: *Comparison of EINOx values for the M1.6 engine of CU : the kinetic evaluation is depicted by the black solid line compared to the NASA methods (blue sold line) and the Boeing Fuel Flow method BFFM (brown solid line). NAU P3/T3 method are depicted by the green solid and magenta dashed lines. The regimes' Mach number is shown for reference as a red long dashed line.*

4. CONTRAIL MODELLING

To simulate the contrails plume behind the E-19 Aeolus M1.6 plateform, 3D simulations are carried

out using the compressible Navier-Stokes solver with multi-species CHARME integrated in the CEDRE numerical code [13]. This code is using numerical methods based on cell-centered finite-volume approach on unstructured grids. A first RANS simulation is carried out to get the short-range plume behind the aircraft such as done in [14], then a 3D temporal LES simulation is used to age the plume.

To study the hot and turbulent exhaust of aircraft engines, a realistic configuration is needed. The CAD of the E-19 Aeolus bizjet was delivered by Cranfield University and presented on the Figure 4. For this configuration, the aim is to study the plume behind the engine for a plane during the supersonic cruise.
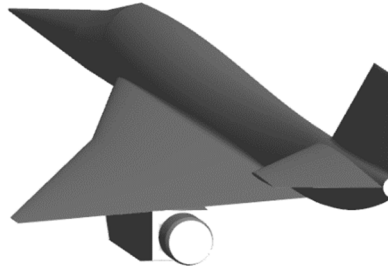

Figure 4. CAD of half the E19 Aeolus bizjet

The computational domain is defined by a box containing half of the aircraft geometry. One of the box faces is set as a symmetry plane. To limit the effects of the boundary on the flow, the other boundaries of the box are set far from the aircraft. The extension of the domain is around 10 spans before the aircraft and 20 spans behind the aircraft. Both lower and upper boundaries of the box are set to 20 spans. Inside the box, the aircraft is oriented along the x axis. The Table 1 presents the computational domain dimensions for the simulations carried out for this configuration. The span b of the E-19 Aeolus bizjet is 14.6 m.

Table 1. Computational domain dimensions

L_x	$[-10\,b, 20\,b]$
L_y	$[0, 20\,b]$
L_z	$[-20\,b, 20\,b]$

For the supersonic cruise, the reference altitude and the Mach number are respectively set to $h = 16339\,\text{m}$ and $M = 1.6$. The total temperature and total pressure are respectively $T_{0,a} = 327.7\,\text{K}$ and $P_{0,a} = 0.409\,\text{atm}$. Thus, the static conditions for the ambient atmosphere are: $T_a = 216.73\,\text{K}$ and $P_a = 9750\,\text{Pa}$. The wind velocity is then $\left\|\vec{V}_a\right\| = 472.16\,\text{m/s}$.

For the engine, a wall condition is imposed except for the entry for which a supersonic outlet condition is applied and for the exit for which the static temperature, the static pressure and the velocity are applied. The Figure 5 illustrates the boundary conditions for the engine. A wall condition is also imposed for the other parts of the aircraft.
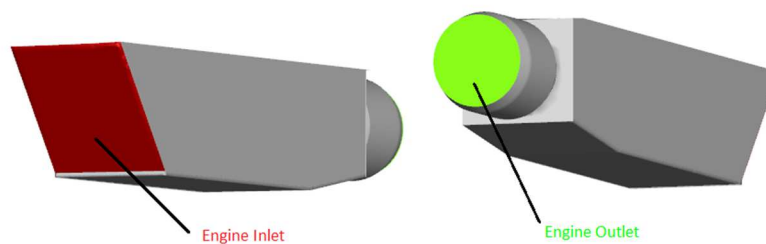

Engine Inlet

Engine Outlet

Figure 5. Boundary conditions for the engine

To avoid large computational time and to correctly capture the interaction between the wing tip vortex and the jet during the jet phase, the mesh needs to be optimised: refined in the area of interests, where

detailed physical must be captured and coarse elsewhere. To distinguish those zones, a mesh adaptation technique using the Feflo software [15] is performed. The parameter used for optimization is defined by:

$$V_t = \sqrt{\sum_j \left(V_j - V_{j,a}\right)^2} + \max(|K - K_a|, K_a), \tag{1}$$

with $V_{j,a}$ the j component of the upwind velocity and K_a the turbulent kinetic energy of the ambient atmosphere. This parameter takes into account two terms. The first one characterizes the velocity regarding the upwind flow. The second measures the impact of the turbulent kinetic energy in the plume compared to the ambient one. For the initial mesh, a small area around the aircraft is refined. After the first refinement steps, twos refined zones appear. The first one corresponds to plume behind the aircraft. Another refined zone corresponds to the different shockwaves that are created due to the aircraft moving at supersonic speed. Indeed, the velocity flow is strongly impacted by the shockwave which explains the mesh adaptation in those areas. The higher the complexity, the more the mesh is refined. In other regions inside the box, the mesh is coarser when the mesh adaptation is used than for the initial mesh.

For the contrails simulation, the ambient temperature and pressure are chosen to simulate the conditions encounter at tropical latitudes (Table 2), for which a sensitivity study (not shown here) shows the highest likeliness for contrail formation. The Emission Indices are presented in Table 3. For the NO$_x$, the repartition between NO and NO$_2$ is calculated directly using: $Y_{NO_2}/Y_{NO} = 0.0424$. For OH and O$_2$, the molar fraction imposed at the engine exit are from 0. Finally, N$_2$ is added to complete the mixing.

Table 2. Ambient meteorological condition used for the simulation

Latitude	Altitude (m)	P_a (Pa)	T_a (K)	$X_{H_2O,a}$ (ppmv)	RH (%)	RH$_{ice}$ (%)
Tropical	16780	9750	195.3	7.9	46.9	100

Table 3. Emission Indices at the exhaust core in g/kg fuel

NOx	CO	CO_2	H_2O	SO_2	SO_3	H_2SO_4
$1.71\ 10^1$	$4.85\ 10^{-1}$	$3.04\ 10^3$	$1.28\ 10^3$	$7.52\ 10^{-1}$	$9.84\ 10^{-3}$	$2.72\ 10^{-2}$

The mass fraction of soot particles is fixed to: $Y_{soot} = 9.34\ 10^{-6}$. This value is calculated by estimating that the UHC emissions correspond to soot emissions. The radius of soot particles and their density are missed to complete the model. Two cases are studied corresponding to two soot radius and corresponding density. The data for those two different cases are resumed in Table 4. Finally, for each case, the relative humidity over ice RH_{ice} is fixed to 100 %.

Table 4. Emission soot parameters

Case	r_s (nm)	ρ (kg/m^3)	$N_s [\#/m^3]$	Reference
Fahey et al.	9	900	$4.76\ 10^{14}$	0
Pueschel et al.	90	1600	$2.68\ 10^{11}$	0

The Figure 6 presents ice crystals data after the exhaust for the 2 cases presented in Table 4. The number of ice crystals is several orders of magnitude higher for the case with data from [16]. which is due to a far higher value of soot emission. For each case, this number remains constant for times higher than 0.5 s after the exhaust. The mean ice crystal radius for the case with data from [17] increases really fast and is almost constant after 0.2 s after the exhaust. For the other case, the growth is quite slower and the mean ice crystal radius keeps growing even far from the aircraft. But for both cases, the IWC tends to the same value which means that the same amount of ice is spread on different sizes of soot particle resulting in different mean values for ice crystal radii. The mean activation fraction is lower for the case with data from [16] and is almost constant at the end of the RANS simulation, contrary to the other case.
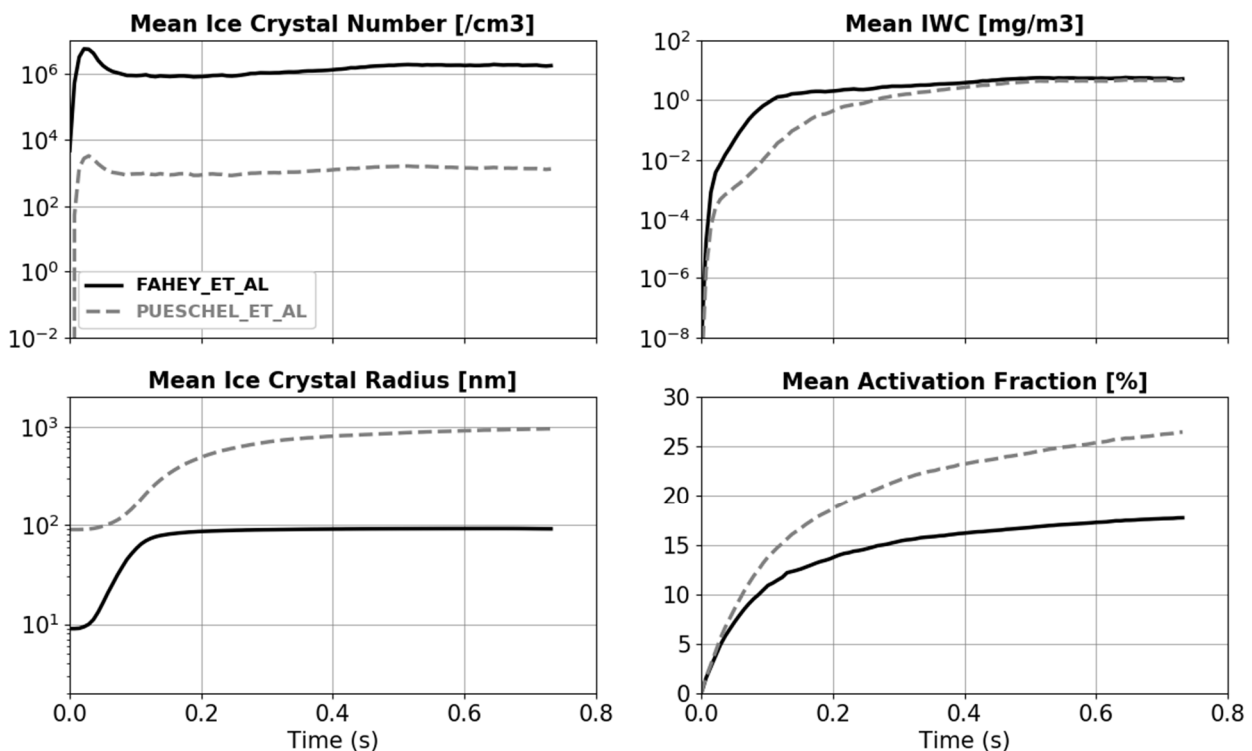

Figure 6. Mean ice crystal number, mean ice water content, mean ice crystal radius and mean activation fraction versus physical time behind the aircraft for the 2 cases presented in Table 4

In order to age the contrails, a RANS/LES methodology has been developed. First, the solution from the previously described RANS simulation must be interpolated. A cut at the end of the mesh is performed and symmetrized to get the effect of the counter-rotating vortex pair. It is important to note

that as periodic conditions will be applied on the two faces of the box in the longitudinal direction, the axial velocity gradients must be negligible in the cut that is performed, meaning that the vortex regime has started. Second, to trigger the Crow instability, turbulent fluctuations due to the jet and in the ambient atmosphere are computed and superimposed on the RANS interpolated mean field. Third, the LES domain extends on around 400 m vertically. For the tropics, the ambient temperature is assumed according to the standard profile to be equals to 195.3 K and constant into the domain but a vertical gradient is apply for pressure to simulate the stratification. In the low stratosphere, the Brunt-Väisälä frequency (N) is directly fixed with the temperature. In our case, in the tropic latitudes we fixed $N = 0.022 \ s^{-1}$.

The evolution of the global contrail shapes for both cases are respectively presented in Figure 7. To obtain this shape, a blanking is applied so only cells containing at least 1000 ice crystals/m^3 is shown. As the contrail is aging, a large part of the ice crystals are trapped in the two vortices and carried down. Some ice crystals are also transported slightly higher that the initial position of the soot particles. The evolution of the contrail shape is quite different when using the data from [16] and from [17] even for short times. Indeed, when using the data from [17] after 3s of simulation, the contrail remains globally cylindrical. When using the data from [16] some lateral lobes are created and the contrail becomes largely asymmetrical.

a)
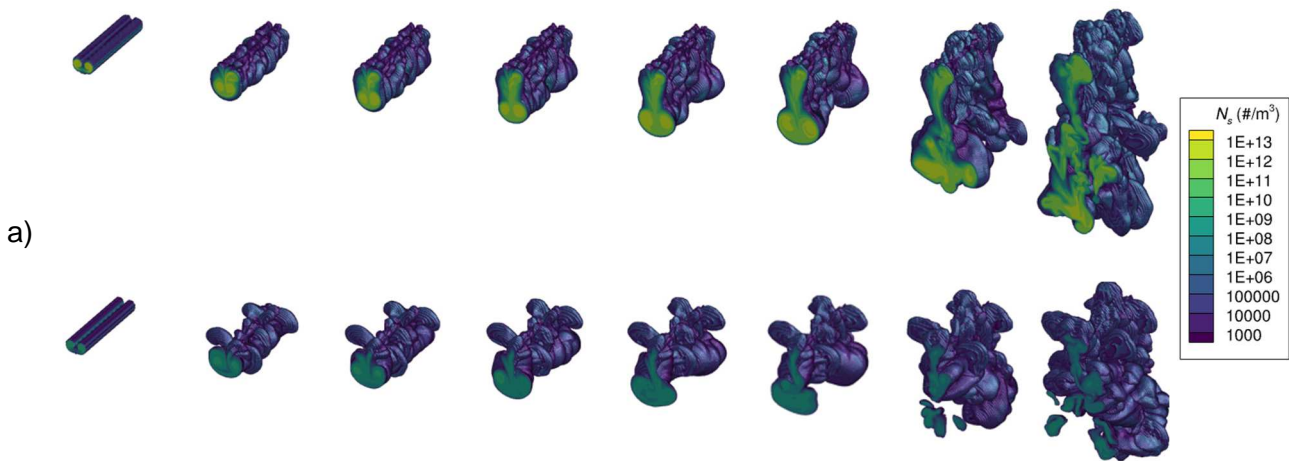
b)

Figure 7. Evolution of the contrail shape with data from [16] (a) and from [17] (b) versus time: 0 s, 3 s, 6 s, 9 s, 12 s, 15 s, 30 s, 60 s

Table 5 summarized the contrail's characteristics after 2 min of aging. The IWC distributions in the contrail for both cases show a strong peak around 0.3 mg/m^3 after 2 min and interpolation were performed to estimate the mean IWC after 5 min, around 0.1 mg/m^3 and 83-84 µg/m3 after 15 minutes of aging (not shown).

Table 5. Contrail data after 2 min aging

	ΔY (m)	ΔZ (m)	A_{yz} (m^2)	$m_{ice,\Delta x=1m}$ (g)	$\overline{IWC}$ (mg/m^3)	$N_{s,max}$ (#/m^3)	$D_p(N_{s,maxi})$ (µm)	IWC_{peak} (g/m^3)
Fahey et al.	150	250	$1.15 \ 10^4$	2.31	0.20	$5.82 \ 10^{12}$	0.185	0.31
Pueschel et al.	180	230	$1.26 \ 10^4$	2.34	0.19	$3.16 \ 10^9$	2.250	0.31

5. CLIMATE EFFECTS

The model for ozone and related chemical tracers, version 3 (MOZART-3) is a 3D-chemistry transport model (CTM) that has been used for an extensive range of different applications, like studying the

impact of El Niño and La Niña events on the structure of the middle atmosphere [18], forecast analysis of the ozone hole over Antarctica [19], evaluation of Ozone Depletion Potentials for n-propyl bromide [20], as well as various aspects of the impact of aircraft NO_x emissions on atmospheric composition [21, 22, 23].

The model configuration used in this study comprises a T42 (~ 2.8° × 2.8°) horizontal resolution with 60 hybrid layers, from the surface to 0.1 hPa. The transport of chemical compounds is driven by the meteorological fields from the European Centre for Medium Range Weather Forecast (ECMWF), 6-h reanalysis ERA-Interim data for the year 2006. The 2050 gridded surface emissions (anthropogenic and biomass burning) were determined by Integrated Assessment Models (IAMs) for the business-as-usual scenario of the Representative Concentration Pathways, RCP 4.5.

The core of the study here constitutes the base case scenario developed for the SCENIC project, S5 a mixed fleet scenario, where part of the subsonic aircraft is replaced by 501 supersonic aircraft. The supersonic fleet is assumed to be operated at Mach 2, with 250 passengers, a maximum range of 5500 NM, and a cruise altitude from 17 to 20 km. In addition, to validate the base case supersonic responses in our chemistry models the reference experiment had to also be performed, and that was the SCENIC S4 scenario comprising a subsonic fleet only. The inventories used here are for the year 2050, and emissions of aircraft NO_x are calculated to be 2.3 Tg(N) yr^{-1} and 2.2 Tg(N) yr^{-1} for scenarios S5 and S4, respectively.

A set of sensitivity experiments was performed to assess the response of aviation O_3 to different emission indices. For this purpose, we have combined the SCENIC S5 inventory with scaled supersonic NO_x emissions (Figure 8).
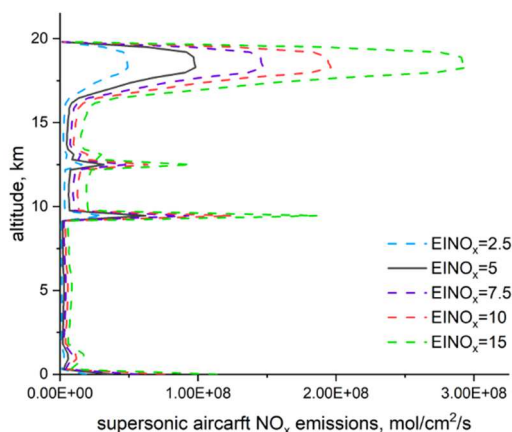

Figure 8: Aircraft NOx emission (mol/cm2/s) according to the altitude height as introduced in MOZART

Aircraft NO_x emissions can either increase or decrease O_3, depending on the ambient environment that is the resultant of the relative balance of NO_x, HO_x, and halogen radicals in the background atmosphere. NO_x in the troposphere produces ozone in the presence of peroxy radicals and sunlight, while in the stratosphere it causes ozone depletion through the catalytic NO_x cycle (Figure 9). A set of sensitivity experiments was performed to assess the response of aviation O_3 to different emission indices. The peaks of the supersonic ozone destruction, as modelled by MOZART-3, varies between -45.6 ppb and -134.5 ppb for EI(NOx)= 5 and 15, respectively.
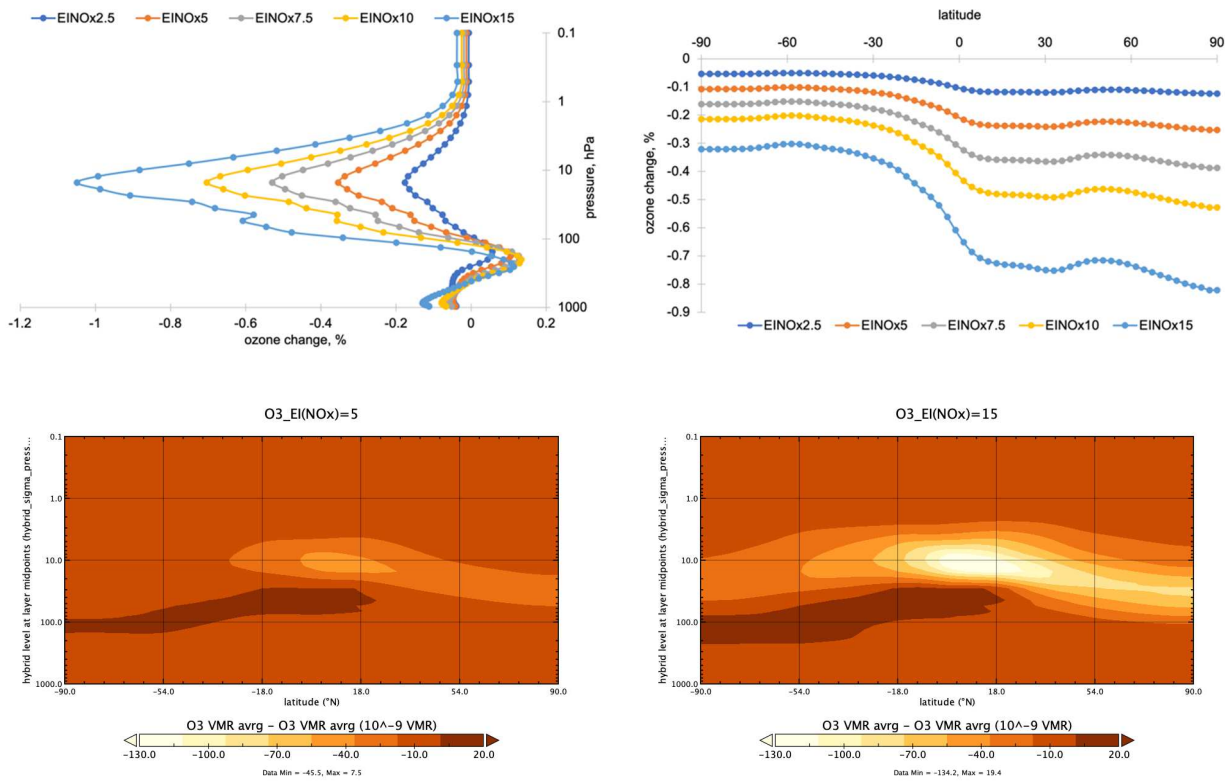
Figure 9: *Aircraft The ozone changes for various emission scenarios, as modelled by MOZART-*

The destruction of ozone is observed to be larger when the emission index for NO_x increases (Figure 10), and it is consistent with other studies. However, different models derive different sensitivities, here MOZART-3 calculates factor of 3.5, while EMAC shows factor of 5.4 over the $EI(NO_x) = 5$ to 15 range. The ozone response becomes less efficient with increasing NO_x emissions (Figure 10). This might have a potential importance for climate/emissions metrics, like e.g., Global Warming Potential.
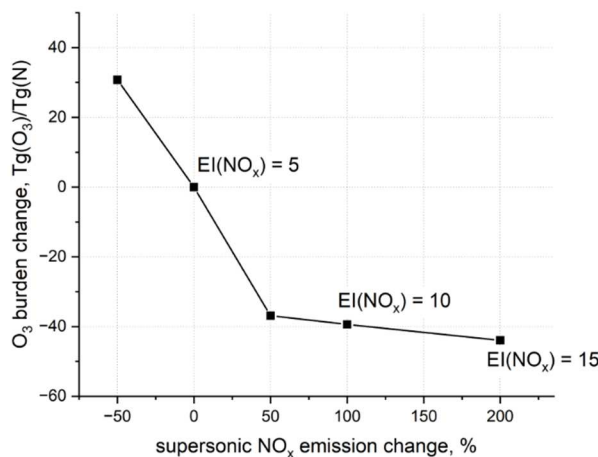

Figure 10: The normalized ozone burden changes to varying supersonic NO_x emissions, as modelled by MOZART-3.

The background conditions play an important role in aviation ozone response, in supersonic ozone too, the cleaner the background the smaller the ozone destruction is observed (Figure 11) Reducing anthropogenic surface NO_x emission by 50% reduces the ozone depletion by around 20%. The ratio of the changes of ozone to different $EI(NO_x)$ ranges remains stable under different background conditions though.
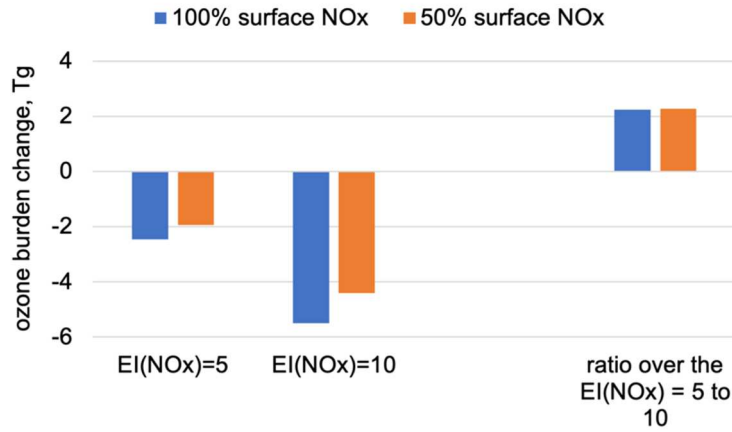
Figure 11: *The total ozone change induced by different supersonic and surface NO_x emissions, as modelled by MOZART-3.*

The calculation of the instantaneous radiative forcing (IRF) of atmospheric concentration changes of water vapour and ozone, linked to supersonic traffic, was performed using the Suite Of Community RAdiative Transfer codes, SOCRATES [23]. This is the off-line version of the radiation scheme used by the UK's Met Office. The background meteorology used in SOCRATES is based on monthly climatological data for H_2O, temperature and surface albedo from ECMWF (Simmons and Gibson, 2000) on a 2.5° × 2.5° regular latitude/longitude grid and 23 layers in the vertical extending up to 1 hPa. Solar zenith angles and day lengths at the middle of the month are used to represent shortwave (SW) radiation averages for each month, while the diurnal cycle is approximated by a Gaussian integration of 5 solar zenith angles. Annual average change in instantaneous radiative forcing (RF) of supersonic O_3 and H_2O calculated at the tropopause are 2.2 and 64.6 mW m^{-2}, respectively (Figure 12).
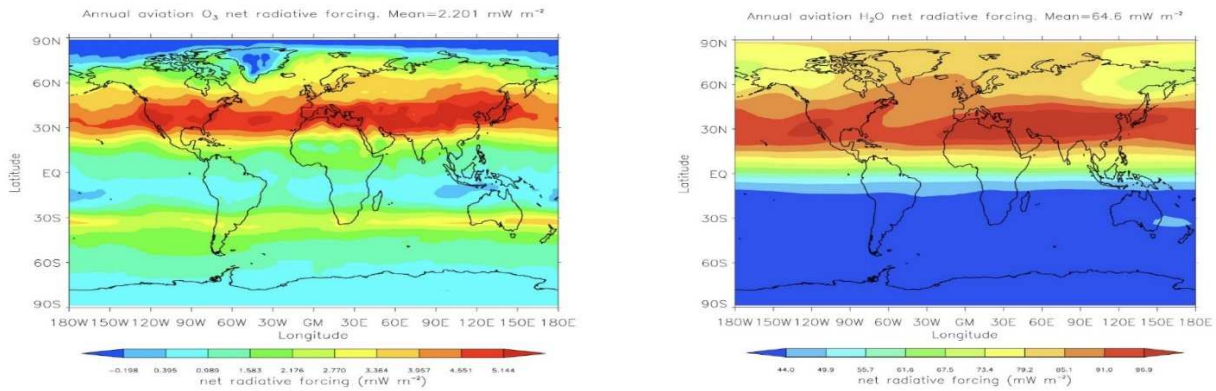

Figure 12: *Annual supersonic aviation ozone (top) and water vapour (bottom) net radiative forcing (mW m^{-2}), as modelled by MOZART-3 and SOCRATES.*

For a comparison, recently, [24] reported 3.8 and 41.9 mW m^{-2} for stratospheric-adjusted O_3 and H_2O RFs. The pattern of ozone RF responses does not change with different sizes of supersonic aircraft NO_x emissions. However, the greater NO_x emissions result in greater ozone RF (Figure 13) and 3 times more NO_x induces 4 times stronger ozone RF response, as modelled by MOZART-3 and SOCRATES.
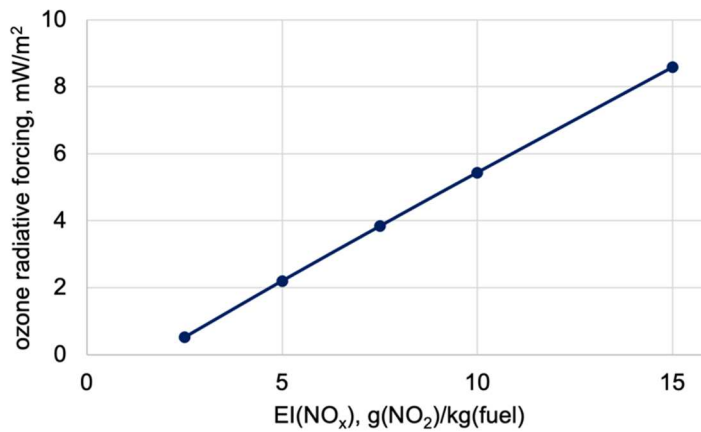
Figure 13: *Annual average change in ozone radiative forcing (mW/m²) as a function of supersonic NOₓ emissions levels, as modelled by MOZART-3 and SOCRATES.*

6. CONCLUSION

Potential future supersonic fleet composed of two categories of supersonic aircraft concepts and associated engines (100 PAX with four engines and bizjets with two engines) have been evaluated with respect to their potential effects on climate in 2050. Emission indices of various types, such as NO_x, CO, CO_2 and SO_x are determined from the more detailed engine studies provided by the SENECA engine team. NOx emissions indexes (20-25 g/kg fuel) are correlated with the fuel/air ratio, which is consistent with the findings also for the ICAO points. EI_SO2 is close to 0.8 g/kg which is a reasonable result, given that sulphur primarily produces SO2 as a pollutant. The EINOx were calculated by the P3T3 method for each of the four stages (take-off, subsonic climb, supersonic climb, supersonic cruise) of the flight profile, and compared to the values obtained with the CANTERA model data. Additionally, EINOx were calculated in accordance to NASA model [12], which is quite well correlated with P3T3 results. Analysis of the obtained results demonstrated, that the influence of relative humidity on emission indices is insignificant.

Contrail 3D characteristics are assessed along with a novel RANS/LES coupling approach allowing simulating the contrails during the jet and vortex phases. Contrails formation and evolution in the jet phase have been simulated for the 2 cases using to different soot EIs. The mean ice crystal radius for the case with high EI_soot increases really fast and is almost constant after 0.2 s after the exhaust. For the other case, the growth is slower and the mean ice crystal radius keeps growing even far from the aircraft. For both cases, the IWC tends to the same value which means that the same amount of ice is spread on different sizes of soot particle resulting in different mean values for ice crystal radii. The IWC distributions in the contrail for both cases show a strong peak around 0.3 mg/m³ after 2 min and interpolation were performed to estimate the mean IWC after 5 min, around 0.1 mg/m³ and 83-84 µg/m3 after 15 minutes of aging.

Finally, the chemical impacts and associated radiative forcing of NOx on stratospheric and tropospheric ozone and water vapor are modelled with the MOZART global climate model. Aircraft NO_x emissions can either increase or decrease O_3, depending on the ambient environment that is the resultant of the relative balance of NO_x, HO_x, and halogen radicals in the background atmosphere. A set of sensitivity experiments was performed to assess the response of aviation O_3 to different emission indices. The peaks of the supersonic ozone destruction, as modelled by MOZART-3, varies between -45.6 ppb and -134.5 ppb for EI(NOx)= 5 and 15, respectively. Annual average change in instantaneous radiative forcing (RF) of supersonic O_3 and H_2O calculated at the tropopause are 2.2 and 64.6 mW m^{-2}, respectively.

7. Copyright Statement

The authors confirm that they, and/or their company or organization, hold copyright on all of the original material included in this paper. The authors also confirm that they have obtained permission, from the copyright holder of any third party material included in this paper, to publish it as part of their paper. The authors confirm that they give permission, or have obtained permission from the copyright holder of this paper, for the publication and distribution of this paper as part of the ICAS proceedings or as individual off-prints from the proceedings.

References

[1] Goodwin, D.G., Moffat, H.K., Schoegl, I., Speth, R.L. and Weber, Bryan W. Cantera: An object-oriented software toolkit for chemical kinetics, thermodynamics, and transport processes. https://www.cantera.org, 2023. Version 3.0.0. doi:10.5281/zenodo.8137090.

[2] Saboohi, Z., Ommi, F., Fakhrtabatabaei, A., Development of an augmented conceptual design tool for aircraft gas turbine combustors. Int. Jnl. of Multiphysics 10, 1, (2016).

[3] A. M. Starik et al.. Impact of Operating Regime on Aviation Engine Emissions, Journal of propulsion and PoweVol. 29, No. 3, May–June 2013

[4] Dagaut, M. Cathonet. "The ignition, oxidation, and combustion of kerosene: A review of experimental and kinetic modelling". Progress in Energy and Combustion Science 32 48–92, 2006

[5] Luche, J.: Obtention de modèles cinétiques réduits de combustion. Application à un mécanisme du kérosène, Universite d'Orleans (2003).

[6] D. Bongartz, A.F Ghoniem, Combustion and Flame 162 52015) 544-553.

[7] Lukachko et al. 1998. Journal of Geophysical Research: Atmospheres, 103 (D13), 16159-16174.

[8] Lopez-Pintor. D., SAF End-Use, Aug. 2022, SAF End-Use, Feb. 2023.

[9] SAE AIR 5715, 2009, SAE Committee A-21, Aircraft Emissions

[10] Duchene N., Synylo K. P3T3 NOx Model of turbofan engine // The International Symposium on Sustainable Aviation, 9 – 11 July 2018: abstracts. – Rome, 2018. – P. 103.

[11] ICAO: Engine Emissions Databank, https://www.easa.europa.eu/domains/environment/icao-aircraft-engine-emissions-databank, version 28C, accessed Juli 2021

[12] N+3 Advanced Concept Studies for Supersonic Commercial Transport Aircraft Entering Service in the 2030-2035 Period – 2011. – P.39

[13] A. Refloch, A. Courbet, A. Murrone, P. Villedieu, C. Laurent, P. Gilbank, J.Troyes, L. Tesse, G. Chaineray, J-B. Dargaud, E. Quemerais and F. Vuillot, Cedre Software, *Aerospace Lab*, no. 2, 2011

[14] J-C. Khou, Modélisation des traînées de condensation par interaction entre l'aérodynamique, la cinétique chimique et la microphysique. Mécanique des fluides [physics.class-ph]. Université Pierre et Marie Curie - Paris VI, 2016. Français

[15] A. Loseille, F. Alauzet, A. Dervieux and P. Frey, Achievement of second order mesh convergence for discontinuous flows with adapted unstructured mesh adaptation, in AIAA conference, 2007

[16] D. Fahey, E.R. Keim, K. A. Boering, C. Brock, J. Wilson, H. Jonsson, S. Anthony, T. F. Hanisco and P. Wennberg, Emission Measurements of the Concorde Supersonic Aircraft in the Lower Stratosphere, *Science*, vol. 270, pp. 70-74, 1995

[17] R. F. Pueschel, K. A. Boering, S. Verma, S. D. Howard, G. V. Ferry, J. Goodman, D. A. Allen and P. Hamill, Soot aerosol in the lower stratosphere: Pole-to-pole variability and contributions by aircraft, *Journal of Geophysical Research*, vol. 102, no. D11, pp. 13,113-13,118, 1997

[18] Sassi, F., Kinnison, D. E., Boville, B. A., Garcia, R. R., Roble, R. (2004). Effect of El Niño southern oscillation on the dynamical, thermal, and chemical structure of the middle atmosphere. Journal of Geophysical Research 109, D17108.

[19] Flemming, J., Inness, A., Jones, L., Eskes, H. J., Huijnen, V., Schultz, M. G., ... & Brasseur, G. (2011). Forecasts and assimilation experiments of the Antarctic ozone hole 2008. Atmospheric

Chemistry and Physics 11,1961-1977.

[20] Wuebbles, D. J., Patten, K. O., Wang, D., Youn, D., Martínez-Avilíes, M., & Francisco, J. S. (2011). Three-dimensional model evaluation of the ozone depletion potentials for n-propyl bromide, trichloroethylene and perchloroethylene. Atmospheric Chemistry and Physics, 11, 2371–238.

[21] Skowron, A., Lee, D. S., De León, R. R., Lim, L. L., & Owen, B. (2021). Greater fuel efficiency is potentially preferable to reducing NO_x emissions for aviation's climate impacts. Nature Communications, 12(1), 1-8.

[22] Skowron, A., Lee, D. S., & De León, R. R. (2015). Variation of radiative forcings and global warming potentials from regional aviation NO_x emissions. Atmospheric Environment, 104, 69–78 (2015).

[23] Skowron, A., Lee, D. S., & De León, R. R. (2013). The assessment of the impact of aviation NO_x on ozone and other radiative forcing responses - the importance of representing cruise altitudes accurately. Atmospheric Environment, 74, 159-168.

[24] Manners, J. and Edwards, J. M. and Hill, P. and Thelen, J.-C., 2015: SOCRATES (Suite Of Community RAdiative Transfer codes based on Edwards and Slingo) Technical Guide. Met Office, UK. Code available at: https://code.metoffice.gov.uk/trac/socrates.

[25] Zhang, J., Wuebbles, D., Kinnison, D., & Baughcum, S. L. (2021). Stratospheric Ozone and Climate Forcing Sensitivity to Cruise Altitudes for Fleets of Potential Supersonic Transport Aircraft. Journal of Geophysical Research: Atmospheres, 126(16), e2021JD034971.